Meteorological Results From the Surface of Mars: Viking 1 and 2

S. L. HESS,[1] R M. HENRY,[2] C. B. LEOVY,[3] J. A. RYAN,[4] AND J. E. TILLMAN[5]

We deal here primarily with the surface meteorological data for both Viking landers during the nominal missions (44 sols for lander 1 and 61 sols for lander 2). The diurnal patterns of wind, temperature, and pressure were strongly similar from sol to sol, as was expected in the summer. The chief characteristics of the wind data are that winds were light (a few meters per second), with a complex hodograph at VL-1 dominated by counterclockwise turning of the wind and a simpler hodograph at VL-2 marked by clockwise turning of the wind. This repetitive pattern of wind has begun to break down at VL-2 with advancing season, and several episodes of protracted northeasterly winds have occurred. Some of these are associated with lower than normal temperatures. Examples are given of wind and temperature traces over short periods, illustrating the effects of convection, static stability, and lander interference. We present a theoretical argument based upon the horizontal scale dictated by heating of slopes and upon vertical mixing of momentum to explain the different sense of rotation of the wind vectors at the two sites. Analysis of the semidiurnal pressure oscillation suggests that absorption of solar radiation is an important thermal drive but that convective heat flux from the surface is also significant. The seasonal variation of pressure extending past the end of the nominal missions shows a decrease of pressure to a minimum at $L_s \approx 149°$ with a rapid rise thereafter. This is clearly due to condensation and sublimation of CO_2 on and from the southern polar cap.

INTRODUCTION

The meteorology experiment aboard the Viking Mars landers (VL-1 and VL-2) was designed to measure atmospheric temperature, wind speed, wind direction, and pressure. The scientific objectives have been described previously [*Hess et al.*, 1972]. In brief, the objectives are to obtain information about the local environment and meso-scale and planetary-scale systems and processes, to investigate boundary layer phenomena, and to obtain a better understanding of earth's atmosphere through comparison with the simpler Mars atmospheric behavior.

The instrumentation has been described by *Chamberlain et al.* [1976]. In brief, the temperature and wind sensors are mounted at the end of a boom which was deployed shortly after landing. Figure 1 shows the boom-mounted sensors, while Figure 2 shows the deployed boom on Mars (VL-1 site). In the deployed position the sensors are nominally 1.6 m above the ground, 0.7 m above the top of the lander body, and slightly more than 0.3 m horizontally outward from the closest portion of the lander body. The objective of the deployment was to place the sensors as far as practicable from lander effects. The pressure sensor is mounted underneath the lander body and is the same sensor used to obtain pressure profiles during the parachute phase of entry. It is of the variable reluctance, stressed diaphragm type and measures over the range 0–20 mbar with least digital step about 0.09 mbar. Its measurement accuracy is much better than 0.09 mbar.

The ambient temperature sensor consists of three Chromel-Constantan thermocouples wired in parallel. It is capable of measuring over the entire range of expected Martian temperatures with an accuracy of about ±1.5°C. Wind speed is measured by means of two hot film (platinum) sensors mounted 90° apart in the horizontal plane and maintained at a nominal overheat temperature of 100°C above ambient as measured by a reference temperature sensor. Wind speed accuracy is about ±10% over most of the range (~2–150 m s^{-1}) but degrades somewhat for very light winds. Lander interference, i.e., wind from over the lander, also degrades accuracy, but ground testing indicates that the degradation should not be much in excess of ±10% for the system as a whole. The wind speed sensors also measure wind direction but with a fourfold ambiguity. Selection of the proper quadrant is accomplished by a quadrant sensor, consisting of a heated cylindrical core surrounded by four thermocouple junctions at equal angles and distance about the core. The thermocouples sense the thermal wake from the heated center core. Overall accuracy in wind direction measurement is about ±10°. All electronics, except the bridge circuit for the ambient temperature sensor, are located within the lander body.

The instruments have performed well during the primary mission (from the Mars landing to the solar conjunction period beginning in early November 1976) except for two anomalies. The first concerned the ambient temperature sensor on VL-2 and was observed shortly before launch. The readings exhibited a temperature-dependent error, increasing as lander body temperature decreased. Also, the error gradually decreased after application of power to the electronics, approaching a steady state value after 30–40 min of operation. A series of checkouts was performed during the cruise phase, and it was concluded that the probable cause of the anomaly was a temperature-dependent resistance change somewhere within the electronics. Analysis of the landed data and comparison with the reference temperature sensors on VL-1 and VL-2 and the ambient sensor on VL-1 permitted a suitable correction to be applied. This required that power be on continuously to eliminate the drift. This was done from VL-2 sol 25 onward. (A sol is defined as 1 Martian day, and a VL-2 sol as the number of sols after VL-2 landing. In like manner a VL-1 sol is the number of sols after VL-1 landing.) Because of this anomaly the reference temperature sensor was utilized as the measure of VL-2 atmospheric temperature throughout most of the primary mission. It is much more susceptible to radiation and conduction errors, but corrections for these have been applied, and it is believed to have a residual error of less than ±4°C. The correction to the VL-2 ambient temperature sensor should bring its error to within ±3°C.

The second anomaly involved the VL-1 quadrant sensor. The heater for the sensor core exhibited intermittent behavior on VL-1 sol 45 and failed shortly thereafter. This precluded

[1] Florida State University, Tallahassee, Florida 32306.
[2] NASA Langley Research Center, Hampton, Virginia 23365.
[3] University of Washington, Seattle, Washington 98195.
[4] California State University, Fullerton, California 92631.
[5] University of Washington, Seattle, Washington 98195.

Paper number 7S0459.

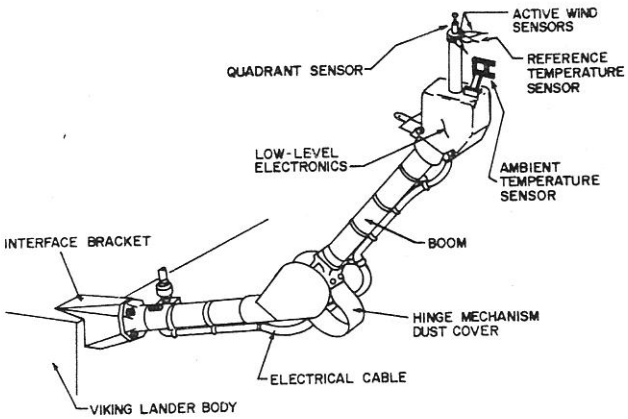

Fig. 1. Schematic diagram of the meteorology boom and sensors.

unambiguous determination of wind direction. Analysis of flight data has revealed that even without power being applied the core remained at a higher temperature than the surrounding thermocouples as a result of solar heating by day and at a lower temperature as a result of infrared radiative cooling by night. The temperature differences are sufficient to be detectable and software modifications to retrieve wind direction information subsequent to sol 45 are being implemented. Although the modifications appear to work well in the low wind speed regime of current operations, the question remains as to how well they will work under the high-wind conditions expected later in the mission.

The on-board lander software was designed to provide a high degree of flexibility in the manner in which meteorology data are taken. One can vary by ground command the rate at which samples are taken, the duration over which a given sample rate is maintained, the serial sequence of sampling rates and duration, the time between sampling sequences, the times and frequencies of sampling initiation, and the total amount of data taken per sol. Prior to landing, preplanned sequences were loaded into each lander. These consisted of modules with durations of about 9, 20, and 39 min spaced nominally 1⅓ hours apart throughout the sol. Intervals between individual samples were 4 and 8 s for the 9-min modules, 4 s for the 39-min modules, and 2 s for the 20-min modules. One complete sequence consisted of 18 modules. Sixteen of these were 9 min long and two, spaced about 12 hours apart, were of longer duration (one being 39 min long, the other 20 min long). The 18 periods were spaced so as to occupy somewhat more than a sol. As a result the pattern of sequences stepped ahead about 1½ hours each sol. This survey mode was adopted in order to define the diurnal cycle while moving long sequences through the sol, a study of fluctuation characteristics at all portions of the diurnal cycle thus being permitted.

Subsequently, extended periods of rapid sampling (about 1-s intervals) were included, for a time, to study boundary layer processes at as high a sampling rate as the system would allow. In addition, various alterations were made in sampling rates, durations, and measurement periods to determine an optimal pattern for sampling the Martian atmosphere. It became evident that the total science return would be maximized by taking samples nearly continuously but at rates slow enough to satisfy mission constraints on total meteorology data. This approach has been followed ever since, except when precluded by mission requirements.

Initially, pressure data were gathered in groups of four samples, 1 s apart, each group being at the start of a module of the other meteorological data. Thus about 18 groups of pressure data were gathered each sol. The pressures within each group of four were almost always the same. Consequently, to maximize the usefulness of the data, this was changed to a pattern in which one pressure sample was taken approximately every 17 min.

VL-1 landed on July 20, 1976, at 22.5°N, and VL-2 landed on September 3, 1976, at 48.0°N. These dates correspond to planetocentric longitudes of the sun, L_s, of 98° and 120°, respectively. Thus both landings were shortly after the beginning of northern hemisphere summer ($L_s = 90°$), and all of the nominal mission data reported here are for summer conditions.

Mission data are being sent to the archives of the National Space Science Data Center as quickly as is feasible. Ultimately, all will be available there to interested scientists.

Winds and Temperatures

At the VL-1 site, little secular change in wind behavior was noted during the first 44 sols on the surface. On sol 45 the quadrant heater, which serves to identify the quadrant from which the wind is blowing, began to exhibit erratic behavior and subsequently failed. The subsequent wind direction data can be recovered, as was noted previously, but as of this writing the data are not yet available. A composite wind hodograph for the first 44 sols is given in Figure 3. The composite was obtained by computing vector mean winds at approximately hourly intervals from individual wind vectors at the corresponding times on all the sols included.

The general behavior of the wind vector is a counterclockwise rotation with one complete rotation per sol. However, localized periods of clockwise rotation are evident. Nocturnal winds are light, generally less than 2 m s^{-1}, and change direction gradually from east to southwest from sunset (about 1910 local lander time (LLT)) to midnight. From midnight through dawn (about 0525 LLT) the wind is roughly from the southwest, the upslope direction at the site (Map M25M 3RMC, prepared by the U.S. Geological Survey for the Viking Program, 1976). This may thus represent a drainage wind. Since the lander is only about 1 km above the lowest point of the Chryse Basin, the earlier nocturnal winds may also represent drainage winds, the gradual shift from east to southwest being related to time after terminator passage, areas to the east cooling earlier.

Wind speed increases following sunrise, reaching a maximum of about 7 m s^{-1} at 1100 LLT, from south-southwest. Wind direction remains from the southwestern quadrant throughout the period. This is in contrast to sand drifts and lee deposits which indicate that the much stronger winds required to move granular material at the site are from the northeast [*Mutch et al.*, 1976*a*]. After 1100 LLT, wind speed declines until 1600 LLT, when nocturnal levels are reached. Concurrently, wind direction shifts through south to east-southeast, directions corresponding to the canyon mouth system associated with Valles Marineris. The mouths lie a few hundred kilometers from the VL-1 site, but the canyons are significant topographic features, in both depth and length, and hence could act as wind channels whose effects are felt at the VL-1 site. The data are also in reasonable accord with predictions from general circulation models [cf. *Pollack et al.*, 1976] extrapolated to the surface.

Detailed inspection of the VL-1 hodographs on a sol-by-sol basis reveals small variations between sols, a few moderately large directional changes lasting 1 hour or less between adja-

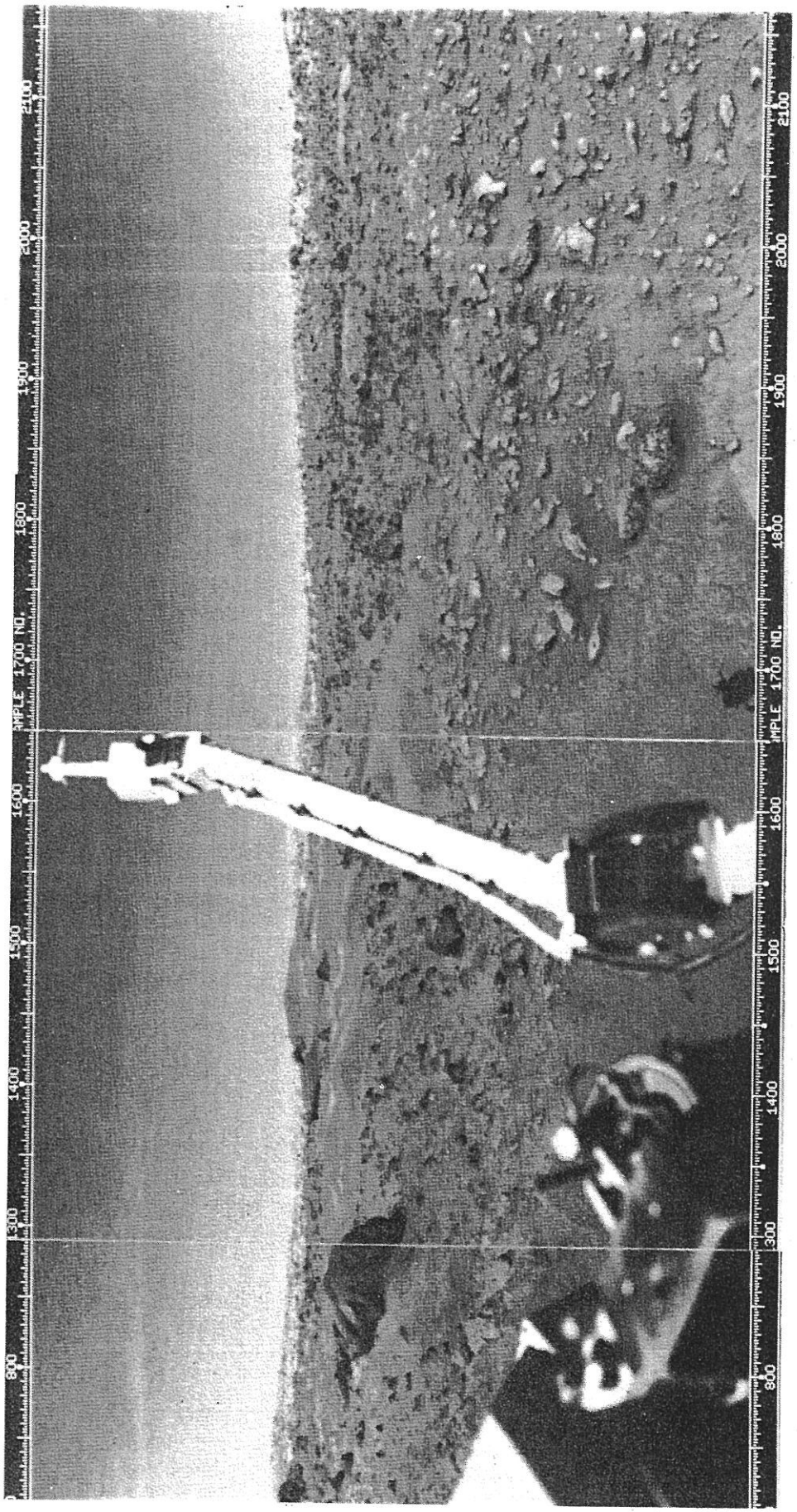

Fig. 2. The meteorology boom and sensors photographed on Mars by a lander camera (VL-1).

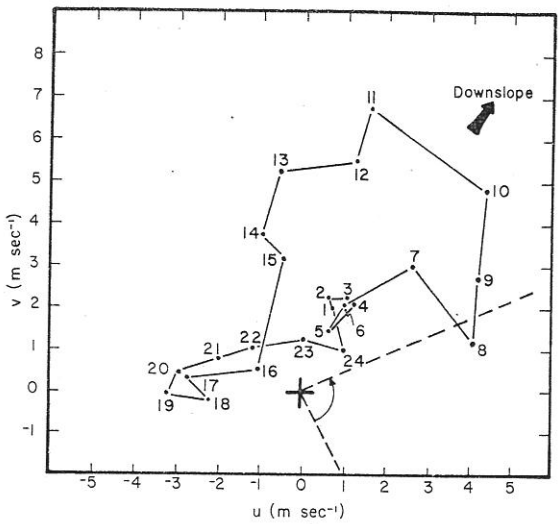

Fig. 3. Mean wind hodograph for the first 44 sols at VL-1. The west-to-east component of the wind is u, and the south-to-north component is v. Thus the wind blows from the origin (marked by a cross) to each plotted point. The number next to each point gives the mean LLT to the nearest hour. Each point represents the vector mean of all observed winds during the first 44 sols measured within 30 min of the indicated time. The sector of lander interference (wind from the lander to the sensors) is bounded by dashed lines connected by an arrow. The heavy black arrow indicates the approximate downslope direction. At VL-1 this ground slope is roughly 0.015.

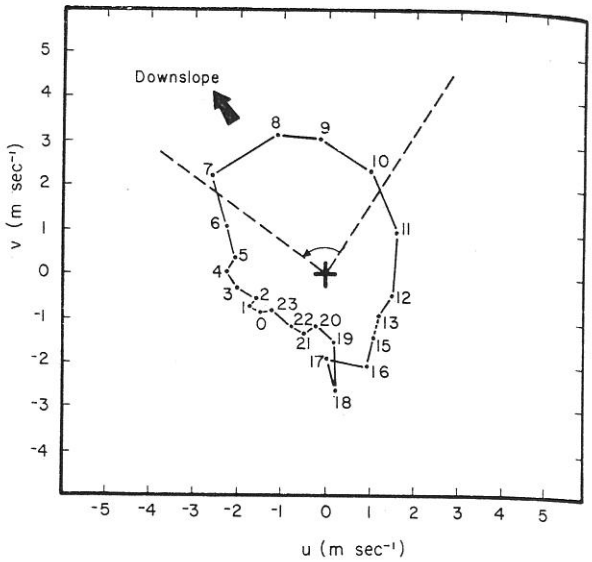

Fig. 4. Mean wind hodograph for the first 50 sols at VL-2 plotted as in Figure 3. A point for 1400 LLT is not shown, since data from only 5 sols are available then; the points for 1300 and 1500 LLT are connected by a dashed line. At VL-2 the ground slope is roughly 0.002.

cent sols, and two small secular trends over the primary mission. The largest short-duration directional change between adjacent sols at appreciable wind speed (>2 m s^{-1}) was an 80° shift which occurred on VL-1 at 1630 LLT each sol over a 3-sol period (sols 20–23). The shift was roughly from east-southeast on sol 20 to south-southeast on sol 21, returning to easterly by sol 23. Only three other changes of similar magnitude (>50°) were observed. No correlation between these shifts and time of day, particular sol, or any of the other measurables was evident.

Two gradual secular trends were observed for VL-1. First, during daylight hours the wind vector at any specific hour turned slowly clockwise from sol to sol, resulting in more southwesterly winds as the mission progressed. At night, however, no such trend was evident. Second, a slight gradual decline in wind speed at night occurred, and the maximum wind for a sol decreased by about 2.5 m s^{-1} during the period. The maximum mean wind typically occurred in the morning (the highest mean speed recorded on any sol being 9.5 m s^{-1}), so that the decline in speed was concurrent with the change in direction. It is premature to ascribe these small secular trends to any specific general or local seasonal changes in circulation.

The wind behavior at the VL-2 site also showed a generally uniform pattern, but significantly more sol-to-sol variation was evident, and several 'events' occurred of which one constituted a dramatic change in wind behavior. A composite hodograph for the first 50 VL-2 sols is given in Figure 4. Unfortunately, owing to the instrument problem on VL-1, the wind data presently available for the two landers do not overlap. The VL-2 composite is distinctly different from that for VL-1 in several ways. First, the wind vector rotates clockwise at the VL-2 site, completing one revolution each sol. Second, all wind directions are represented, whereas for VL-1 no winds from the west through north to east-northeast were observed. Third, the wind speeds are significantly less than at the VL-1 site, particularly during the daytime hours. (Sunrise at the VL-2 site at landing was 0420 LLT, while on sol 61 it was 0459 LLT. The corresponding sunset values are 2017 and 1920 LLT.) Finally, maximum winds are from the southeast versus south-southwest at VL-1. This is in contrast to sand deposits at the VL-2 site which indicate the much stronger winds required to move granular material fare from the northwest [*Mutch et al.*, 1976*b*]. Data at VL-2 during the primary mission were collected for 61 sols. The following discussion and the hodograph are limited to sols 0–50, since during sols 51–61 a dramatic change in the wind behavior was observed. This event is discussed later in this paper.

Nocturnal winds are light as at the VL-1 site and rotate from north to east as the night progresses. Peak wind occurs in midmorning followed by a decay to nocturnal values by late morning. Peak winds are from the southeast, the general direction of Hecates Tholus and Elysium Mons, roughly 1000 km distant. These are the dominant topographic features in the Utopia Planitia area with peaks more than 10 km above the VL-2 site and an apparently monotonic downward slope to that site. The topography at the VL-2 site is not as well known as that at the VL-1 site, but it is possible that the midmorning maximum winds represent drainage winds from the southeastern area.

As was noted above, significant departures from the composite picture, as well as trends, were observed. The magnitude, time of occurrence, and direction of maximum wind on a given sol varied significantly. The largest maximum wind during the first 50 sols was 7.1 m s^{-1}, occurring at 0700 LLT on sol 30 with wind from the east-southeast. The lowest maximum wind was 2.1 m s^{-1}, occurring in the time period 1500–1600 LLT on sol 19 with wind from the north. The largest and most frequent maximum winds on a sol-to-sol basis are from the east-southeast, but a secondary maximum, based on frequency of occurrence and magnitude, occurred with wind from the south-southwest. The complete directional range over which maximum wind occurred on individual sols was from east through south to north, but directions other than east-southeast and south-southwest were quite infrequent and represented instances when wind was light throughout the sol. Times of maximum wind varied from 0400 to 1730 LLT, but

again the maximum occurred most frequently and was largest from 0700–0800 LLT. There is a suggestion of periodicity in the interdiurnal variation of maximum wind speed, but the evidence is inconclusive.

During the early morning hours, particularly from 0500 to 0800 LLT, wind speed gradually increased until approximately VL-2 sols 28–34, where it peaked at values 1.5–2 times those shortly after landing. No wind direction trend was associated with this. Subsequently, wind speed during the same time period decreased to previous values by sols 40–50 and thereafter increased to the event beginning on sol 52.

From 0900 to 1800 LLT the wind speed behavior was distinctly reversed from the early morning period, exhibiting pronounced minima in the period from sol 20 to sol 30 and immediately preceding the event, with pronounced maxima around sols 5–15 and around sols 35–45. No trends in wind direction were correlatable with these changes. These speed variations, particularly during the midafternoon hours, exhibited pronounced quasi-cyclic behavior with a peak-to-peak amplitude of about 2 m s^{-1} and a period of about 23 sols. From sunset through dawn, wind speed varied randomly through the sols except for a pronounced increase on about sol 50 leading up to the event.

Wind direction exhibited several trends through sol 50. From midnight through dawn the wind turned slowly counterclockwise from sol to sol, beginning about sols 20–25, the total turning by sol 50 amounting to 40°–50°. From 0700 through 1200 LLT the wind began a counterclockwise turning about sol 10, shifting about 50° by sol 25, at which point a clockwise turning began. This continued until about sol 50, reaching the original directions. The directional behavior during the afternoon hours was erratic but with some suggestion of a periodic behavior. Oscillation was most pronounced, by far, between 1400 and 1500 LLT, where wind would be from north through east for several sols and then shift to north through west, a total of five such shifts being discernable through sol 50. Wind direction during the nocturnal hours was variable, no trends or patterns being evident.

A dramatic change in diurnal wind behavior began to be evident on sol 51 when wind during the late afternoon hours was from the north-northeast with a diurnal peak from this direction of 5.6 m s^{-1} at 1700 LLT. The same behavior was evident on sol 52. By sol 53 the wind was confined to the sector north through east to southeast, while throughout sols 54 and 55 the wind blew continuously from the northeast with a maximum of 6 m s^{-1}. Figure 5 shows the sol 55 behavior. On sol 56 the wind reverted to its previous behavior and continued in this 'normal' fashion through the remainder of the primary mission (VL-2 sol 61). This event was not accompanied by any definite temperature change. However, it was closely associated in time with increased fluctuation of pressure at both the VL-1 and the VL-2 site. The pressure decline noted throughout most of the primary mission ceased about this time, and it is not known whether or not the pressure fluctuations are directly associated with the wind event. However, it is quite likely that the event represents some type of north polar wave indicative of the approaching autumn and winter seasons. As of this writing (February 1977), several similar events have occurred subsequent to the end of the primary mission. Although these have not as yet been analyzed in detail, it appears that the north polar region is exerting an increasingly dominant influence upon the weather at the VL-2 site, not only with respect to stronger and more northerly winds but also with respect to declining temperatures. The repetitive pattern of northern summer appears to be changing.

As was previously reported [*Hess et al.*, 1976*a*, *b*], the diurnal temperature cycles at both landing sites have been strikingly repetitive from day to day. As is shown in Figure 6, this pattern has continued throughout the primary mission, and thus through most of the Martian summer, with little change except for very gradual seasonal cooling at the VL-2 site. Even the anomalous northeast winds of sols 54 and 55 produced little perturbation of the repetitive pattern, as can be seen by comparing the curves for sols 45 and 55 in Figure 6 (bottom panel).

Figure 7 shows the day-to-day variation of minimum, maximum, and mean ambient temperatures at the instrument height of 1.6 m. Interdiurnal variations are small at both landing sites. Very little seasonal change can be seen at VL-1, but a slow seasonal cooling with a small reduction in diurnal range is apparent at VL-2. Also shown in Figure 7 are the planetary surface brightness temperatures taken from *Kieffer* [1976]. The minimum air temperatures differ only slightly from the surface temperatures. As was expected [*Gierasch and Goody*, 1968], the maximum air temperatures are considerably lower than the planetary surface temperatures.

Variations of temperature, as well as of wind, become increasingly larger in the last few sols of the period, suggesting the approach of a season of greater variations.

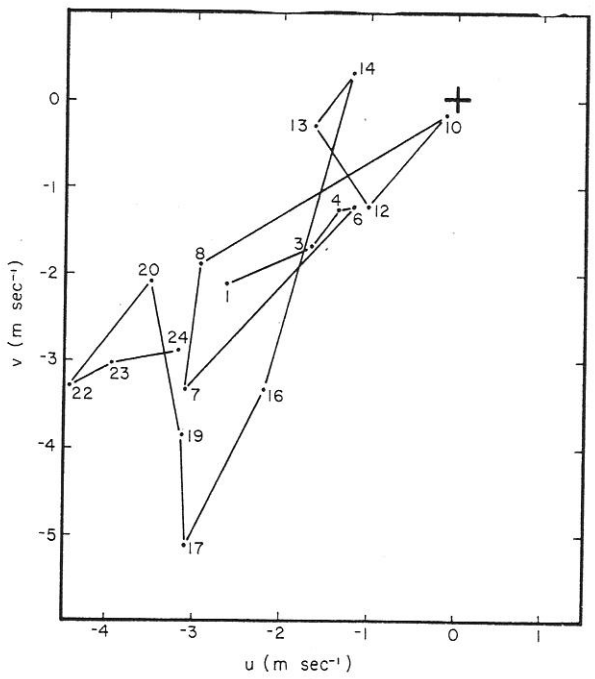

Fig. 5. Wind hodograph on sol 55 at VL-2, at the peak of the only major event during the primary mission. This is plotted as in Figure 3 except that only 1 sol is represented.

TURBULENT CHARACTERISTICS

The planetary boundary layer and the surface layer of planets like the earth and Mars are turbulent, and their fundamentally important characteristics are the static stability and the vertical fluxes of heat and momentum. (For the purpose of this section we take the planetary boundary layer to mean the atmosphere from the surface to the first inversion, several kilometers in daytime, while the surface layer is the shallower layer where the heat and momentum fluxes do not vary significantly from the surface value.) To measure these fluxes directly

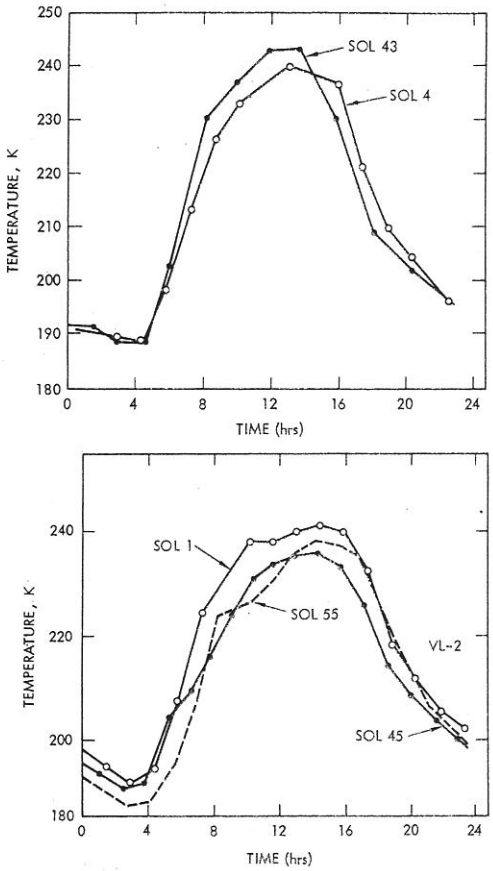

Fig. 6. Diurnal temperature variation at (top) VL-1 and (bottom) VL-2 for sols early and late in the primary Viking mission.

at heights of 1.6 m requires sampling rates of several tens of hertz and three-dimensional measurements.

Since neither three-dimensional measurements nor sampling rates greater than 1.0 Hz are available from Viking, the fluxes and stability can only be inferred indirectly by examining the time series, from statistical properties, or by other indirect means. To aid the reader in understanding the value and the limitations of these data in applications involving both mean and statistical analyses, we present several typical examples of the time series. Some comparisons of the statistics with terrestrial data are also presented.

Continuous time series have been obtained with sampling intervals ranging from 1.0 to 128.0 s and with the number of samples in a module ranging from 16 to 2000. However, modules having less than 64 samples are not generally useful for time series analysis. We have not completed analysis of the time series data because of the demands of the ongoing mission and because of the substantial effort required to validate these series properly for analysis. That work is in progress. To represent the large set of time series, we present a nighttime stable case, a daytime convective case, and an evening transitional case. As a further aid to understanding the data and its limitations a case with interference arising from flow over the lander is given.

Figure 8 is the nighttime stable case. The fluctuations exhibited are similar to the effects on earth of mechanical turbulence generated by roughness elements. The minimum scalar speed is 1.2 m/s (which is above the instrumental threshold), the maximum is 6.5 m/s, and the mean is 3.4 m/s. The wind direction varies between 190° and 225° with a mean of 204°. There is a slight clockwise turning of the wind from the beginning to the end of the record. Temperature data are from the thermocouple system (the prime source of temperature data) and from the wind reference temperature sensor, uncorrected for radiation and conduction errors. These errors can be as high as 8°C. It is therefore essential in using the output of this secondary source of temperatures to correct for radiation and conduction. We are routinely generating both corrected and uncorrected temperatures.

Figure 8 indicates that there is a modest amount of energy in the wind speed and direction spectra with periods of several minutes. The temperature traces are undistinguished except that the two traces diverge toward the end of the record.

Figure 9 is an example of late afternoon convection. The sequence ends about 2.8 hours before sunset. The major variations in wind speed have a period of about 20 min, with significantly less energy in shorter periods. This is due to thermal convection with horizontal scales of the order of several kilometers and is in distinct contrast with the nighttime stable case. In this example there is much better agreement between the two temperature sensors, despite the solar heating of the wind reference sensor, because the wind reference sensor has been corrected for radiation and conduction.

Figure 10 illustrates the transition from strong to decaying convection during late afternoon with a 2-hour module beginning 2.3 hours before sunset. The decay of the low-frequency convective input in the wind speed and direction trace with time is evident along with the almost monotonic decrease in temperature.

We have previously reported a high degree of uniformity of diurnal patterns of wind and temperature from sol to sol in the early part of the mission [*Hess et al.*, 1976*a*] and have taken advantage of that uniformity to calculate the composite values over a 20-sol period as a function of time during the sol. Table 1 compares the module means corresponding to Figures 8, 9, and 10 with the values at the same LLT from the 20-sol composite. The close agreement exemplifies the sol-to-sol uniformity that made it feasible to calculate meaningful composites.

Figure 11 illustrates the effect of lander interference. The wind azimuth trace shows that the wind blew from the lander toward the meteorology sensors near the end of the record. The region of such lander interference for VL-1 is a wind from 246°–332°, and that for VL-2 is a wind from 126°–212°. Lander interference will affect both temperature and wind, but its effects are more readily detected in the temperature traces than in the wind traces owing to the lander's thermal plume.

The entire lander body is a source of heat, but the major heated areas are the two radioisotope thermoelectric generators. They are capable of creating plumes several degrees Celsius above ambient as shown at the end of Figure 11. There are other physically small sources of heat such as the support structure of the meteorology sensor assembly (heated by the sun and by conduction) and the active wind sensors. These primarily affect the readings from the wind reference sensor, when it is downwind of these sources, since it is close to the local sources. The thermocouple sensor is much less affected, since the only structure close to it is the pedestal supporting the wind sensors. This sensor is located such that when the pedestal is upwind of the thermocouples, the wind is blowing from lander to sensor, so that both lander and pedestal interferences are in the same azimuth angle range. This difference in interference effects between the two temperature sensors is of

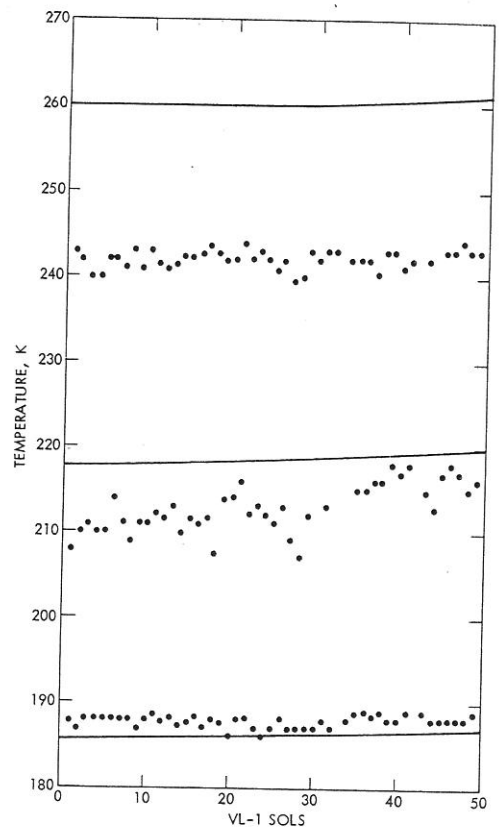

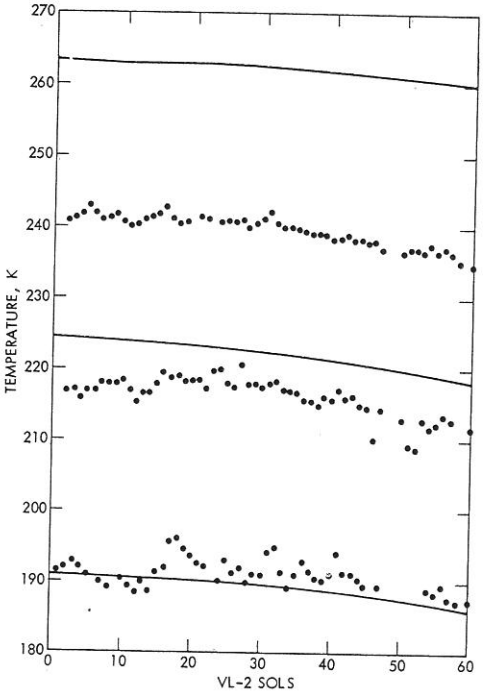

Fig. 7. Maximum, mean, and minimum temperatures for (top) VL-1 and (bottom) VL-2 for each sol of the primary Viking mission. On some sols, one or more of these quantities was in doubt because of winds from over the heated lander, and so no value is shown. Solid lines are maximum, mean, and minimum surface brightness temperatures from *Kieffer et al.* [1976].

particular importance for VL-2, where there is the electronic problem discussed earlier. The process of correcting the thermocouple values for this electronic problem involves comparison with the wind reference sensor readings. For this purpose it was necessary to exclude carefully from the comparison set those wind directions that would produce local as well as total lander effects on the wind reference sensor.

Figure 12 presents the diurnal variation of several statistical parameters for VL-1 sol 3 and the Massachusetts Institute of Technology Round Hill field station site at Buzzards Bay, Massachusetts. The Round Hill data include only data from the wind direction sector which has the most uniform upwind fetch. In the immediate few hundred meters upwind, Round Hill is probably as uniform (except for moisture) as the Viking sites, and it changes to a wooded terrain with a 20-m hill 1.0 km or more from the site [*Cramer et al.*, 1967].

Figure 12 (bottom) compares the gustiness ratio, the ratio of the standard deviation to the mean wind, for the two locations and for a similar range of wind speeds. The Round Hill standard deviations are computed after high-pass filtering at 0.0016 Hz, while the Mars values are computed around a 16-point mean. Since the 16-point mean corresponds to 2 min or less with the sampling intervals used on sol 3, the Mars data generally have smaller standard deviations, in convective conditions, than they would have if the longer periods were included. Note that the gustiness ratios at both sites are quite similar from 0200 to about 1000. After 0600, convection grows in depth, increasing the gustiness ratio until a maximum is reached at about 1400. The diurnal variation of the Round Hill data is smoother than that of the Mars data, since it is a composite of many weeks' data and a greater variety of synoptic situations. Also, the Martian diurnal cycle at VL-1 and VL-2 is probably dominated by thermally generated slope winds, including drainage winds, and by coupling to winds aloft [*Hess et al.*, 1976*a*, *b*] (see next section) at this season. Note that the Round Hill data are dashed during midday due to uncertain or missing data. This is mainly due to the fact that the good wind sector during summer is associated with good weather only during synoptic highs. Since the site is coastal, a sea breeze circulation often opposes the westerly flow during this portion of the day, thereby limiting the sample acquired. Experience at other sites indicates that the Round Hill gustiness is lower than at dry desert sites during low wind speed midday convective conditions.

Figure 12 (middle) compares the standard deviation of azimuth angle for the same two data sets. The lower Mars curve is obtained by computing a standard deviation around a 16-point record mean, while the upper curve is for the standard deviation around the module mean (4–8 records of 16 samples each). Including the lower frequencies essentially doubles the azimuth variations during the convective period. In general, the standard deviation increases with decreasing frequency, almost leveling off as the convective scale is passed, and again increasing as the diurnal variation is included.

Figure 12 (top) illustrates the diurnal variations of temperature variability after the record mean is removed. Note that it increases dramatically around 0600 with the onset of solar heating as the heat flux goes from a small downward value at night to a large upward value during the day. The diurnal variation is similar to that of the azimuth angle variation, and it is possible to compute the heat flux during the unstable portion of the day from 0700 to approximately 1600 [*Tillman*, 1972].

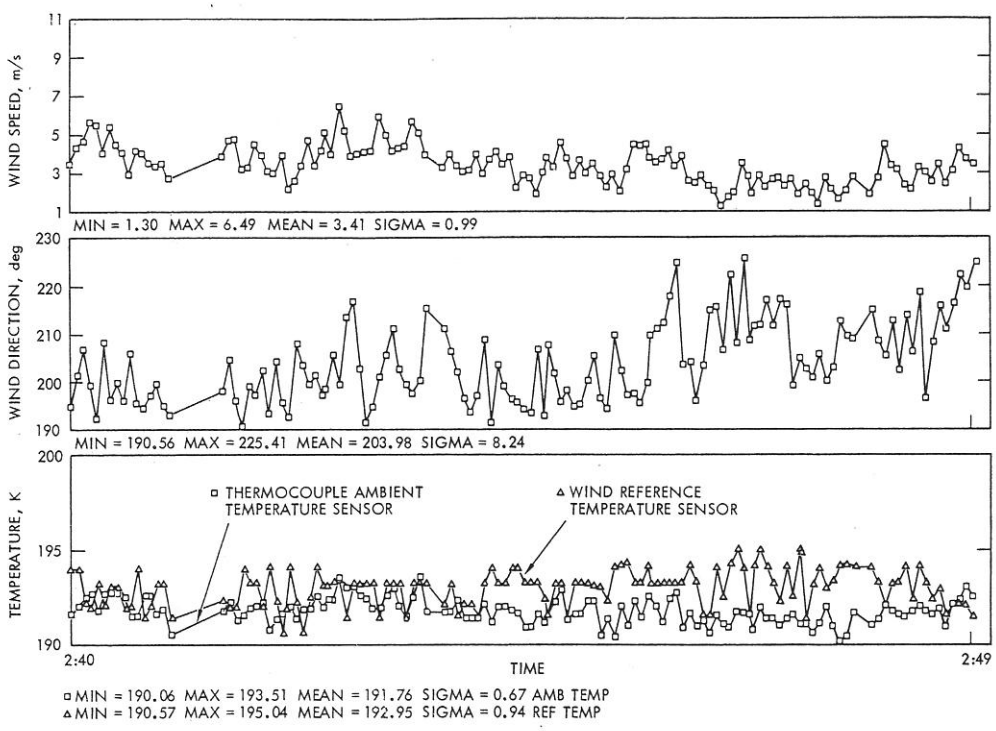

Fig. 8. Nighttime stable case from VL-1 sol 22. This series has a 4-s sampling interval and a total duration of 9 min. The wind reference sensor temperatures are uncorrected. The time scale is hours and minutes.

Interpretation of the Daily Variations of Wind and Pressure

The repeatable daily variations of wind and pressure can be attributed to a variety of diurnal and semidiurnal forcing factors. In general, the wind variations are dominated by processes of smaller scale than the pressure variations, since winds are influenced by the gradient of pressure. A small-amplitude pressure variation acting on a small scale can have more influence on local winds than a much larger amplitude pressure variation acting on a global scale. We believe that the observed pressure fluctuations are primarily planetary in scale for two reasons: (1) the phases of both diurnal and semidiurnal components of the pressure variation are similar at the two sites, and (2) the observed pressure variations would induce much stronger winds than those observed if they had the scale of local topographic variations, for example, the scale of the Chryse basin. Conversely, the winds at both sites seem to be associated primarily with local effects. The wind at both sites is approximately in the local upslope direction in the late after-

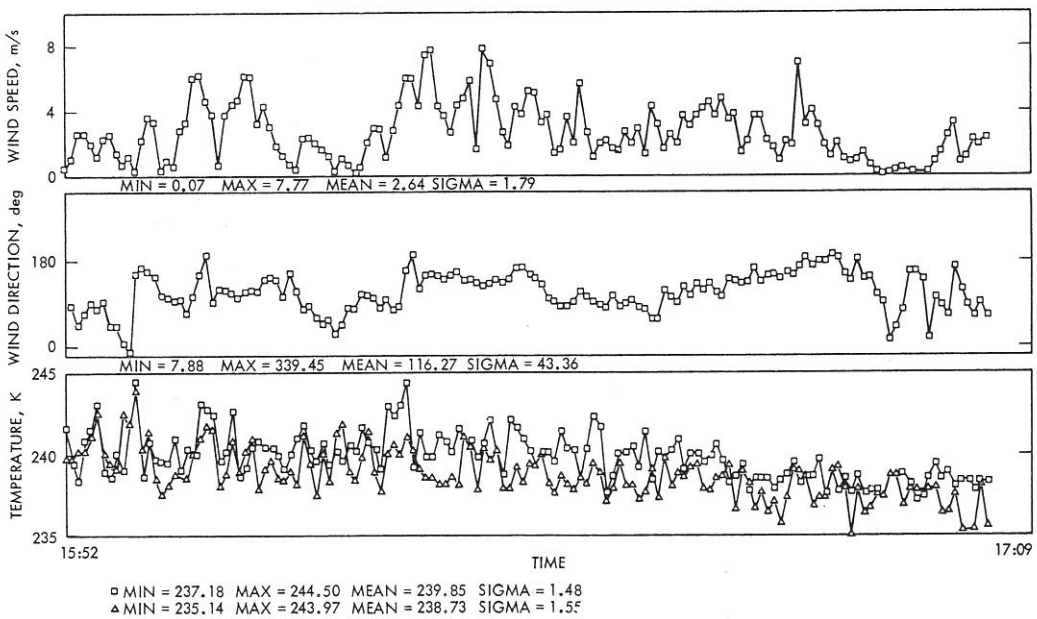

Fig. 9. Late afternoon unstable convective case from VL-1 sol 22. This series has a sampling interval of 32 s and a total duration of 76 min. The wind reference sensor temperatures are corrected. The time scale is in hours and minutes.

TABLE 1. Comparison of Module Mean Data Corresponding to Figures 9, 10, and 11 With the 20-Sol Mean Results at the Same LLT [*Hess et al.*, 1976a]

Source	0240 LLT		0701 LLT		1122 LLT	
	Module Mean	20-Sol Mean	Module Mean	20-Sol Mean	Module Mean	20-Sol Mean
Wind speed, m/s	3.4	2.5	4.0	3.3	6.7	6.8
Wind direction, deg	204	201	240	223	187	192
Temperature, °K	192	190	199	198	234	234

noon and is downslope in the early morning. This property, discussed in greater detail below, is expected for winds under local topographic influence [*Blumsack et al.*, 1973], but it is inconsistent with the variation expected for planetary scale tidal winds [*Zurek*, 1976]. The same separation between planetary scale diurnal pressure variations and local or regional scale daily wind variations occurs on earth [*Chapman and Lindzen*, 1970; *Wallace and Hartranft*, 1969]. Although this separation of planetary effects from local effects on the wind variation is likely to be a very crude approximation, we assume in the present analysis that the observed winds are controlled entirely by local factors while the observed pressure variations, particularly the semidiurnal variation, are entirely planetary in scale.

Wind Models

Two distinct processes have been suggested as drives for local wind oscillations over terrestrial land areas. *Blackadar* [1957] pointed out that the coupling between near-surface winds and those at higher levels varies diurnally as a result of the diurnal variation of the turbulent mixing rate. The influence of such a coupling is suggested by the mean VL-1 hodograph (Figure 3). The winds at the 1- to 2-km level during midafternoon were from the south-southeast at about 20 m/s, at least on the landing sol [*Seiff*, 1977]. The southerly component of the observed winds during midday suggests coupling to the upper-level wind at this time of day. The simplest analytic treatment of this effect is the Rayleigh friction model with a diurnally varying coupling coefficient, and this model will be used here.

The second forcing factor is the diurnally varying pressure gradient associated with the local slope [e.g., *Holton*, 1967]. This factor includes the drainage wind mechanism mentioned earlier. As the boundary layer is heated or cooled almost uniformly along surfaces parallel to the slope, a pressure variation is produced as a hydrostatic consequence of the resulting horizontal temperature variation. The magnitude of this effect is readily shown to be [e.g., *Blumsack et al.*, 1973]

$$\delta \mathbf{G} \approx (gh\delta\Gamma/\bar{T})\ \nabla z \tag{1}$$

where the left side represents the variation of the pressure gradient force induced by lapse rate variation $\delta\Gamma$ occurring through a boundary layer of depth h on a slope ∇z. Other quantities are the gravitational acceleration g and mean temperature $\bar{T}$.

With the Rayleigh friction assumption the wind $\mathbf{u}$ is described by the linearized equation of motion

$$\partial \mathbf{u}/\partial t + f\,\hat{\mathbf{k}} \times \mathbf{u} = \mathbf{G} - d(\mathbf{u} - \mathbf{u}_f) \tag{2}$$

where $\hat{\mathbf{k}}$ is the vertical unit vector, $\mathbf{u}_f$ is a 'relaxation wind' assumed to be approximately equal to the actual wind at the 1- or 2-km level, f is the Coriolis parameter, and d is the Rayleigh coupling coefficient. The quantities $\mathbf{u}$, $\mathbf{G}$, d, and $\mathbf{u}_f$ can be separated into daily mean and diurnal components, denoted by overbars and primes, respectively:

$$(\mathbf{u}, \mathbf{G}, d, \mathbf{u}_f) = (\bar{\mathbf{u}}, \bar{\mathbf{G}}, \bar{d}, \bar{\mathbf{u}}_f) + \mathrm{Re}\,[(\mathbf{u}', \mathbf{G}', d', \mathbf{u}_f')e^{i\omega t}]$$

This separation leads to the steady oscillation component of the solution for the complex amplitude of the diurnal wind oscillation:

$$\mathbf{u} = -\frac{[(i\omega + \bar{d}) - f\hat{\mathbf{k}}\times]}{[(i\omega + \bar{d})^2 + f^2]}\ [\mathbf{G}' - d'(\bar{\mathbf{u}} - \bar{\mathbf{u}}_f) + \bar{d}\mathbf{u}_f'] \tag{3}$$

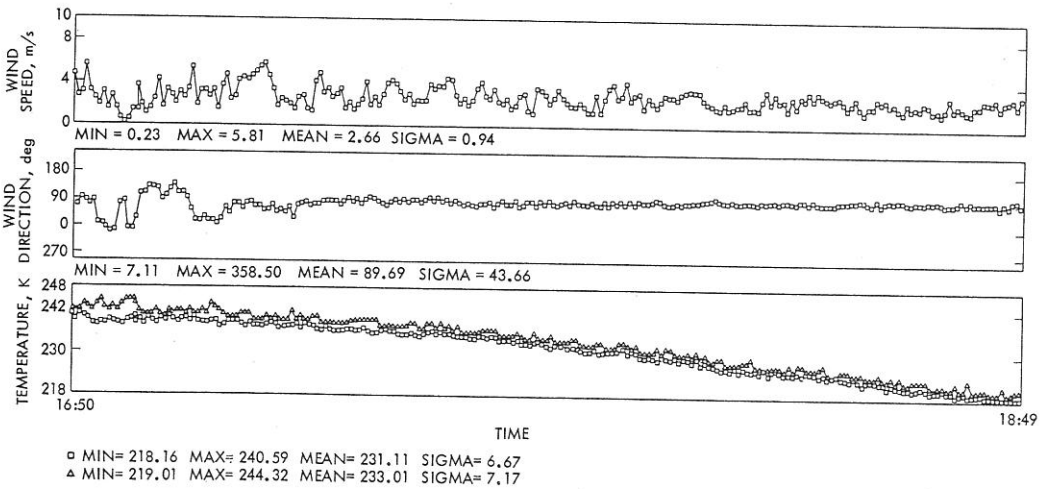

Fig. 10. Evening transitional case from VL-1 sol 30. This series has a sampling interval of 32 s and a total duration of 2 hours. The wind reference sensor temperatures are corrected. The time scale is in hours and minutes.

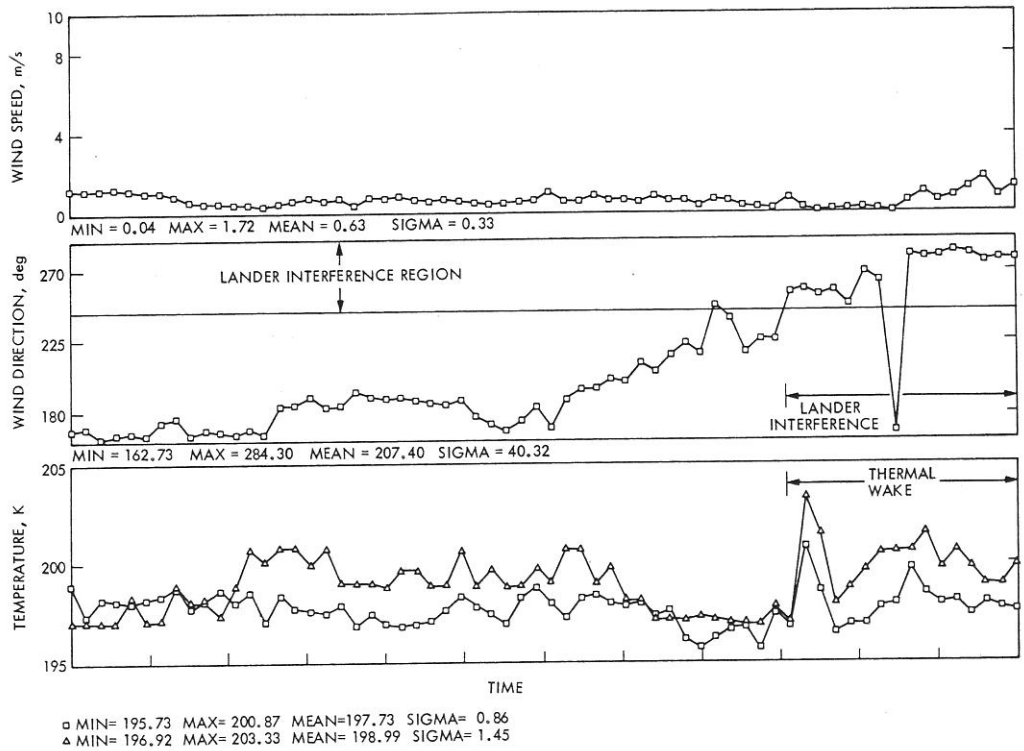

Fig. 11. A case of lander interference from VL-1 sol 29. This series has a sampling interval of 48 s and a duration of 51 min starting at 2310 LLT.

Equation (3) covers many possibilities depending on the magnitude and direction of $\mathbf{G}'$, the magnitude of $\bar{d}$ and d', and the magnitudes and directions of $\bar{\mathbf{u}}_f$ and $\mathbf{u}_f'$. To reduce the range of possible parameter variations to a manageable one, we neglect $\mathbf{u}_f'$ and assume that $\mathbf{G}'$ is given by (1), that is, $\mathbf{G}'$ is assumed to be directed only upslope or downslope. These simplifications are based on the assumption that planetary scale diurnal pressure and wind variations do not strongly affect the diurnal surface wind. Moreover, at the VL-1 site the direction of $\bar{\mathbf{u}}_f$ is taken to correspond to both the observed wind aloft and the slope-induced mean wind, i.e., it is parallel to the topographic contours with low elevations to the right of the flow. Finally, note that the nighttime surface winds are essentially decoupled from the winds aloft; a preliminary analysis combining VL-1 air temperatures and winds and ground temperature estimates from Viking orbiter 1 [*Kieffer*, 1976] suggests that the bulk Richardson number at night is very close to the critical one for the suppression of turbulent exchange across the boundary layer. Hence it is reasonable to assume that coupling vanishes at night. In terms of the Rayleigh friction model this implies that $\bar{d}$ and d' are comparable in magnitude, and we take them to be equal.

With these assumptions the solution hodographs depend on latitude, the relative phase of d' and $\mathbf{G}'$, and the ratio of the coupling factor to the slope-induced pressure gradient:

$$r \equiv |d'| \times |\bar{\mathbf{u}} - \bar{\mathbf{u}}_f| / |\mathbf{G}'|$$

We have explored the parameter ranges $0 \lesssim |\bar{d}| \lesssim 10^{-4}\,\mathrm{s}^{-1}$ and $0 \lesssim r \lesssim 4$ and two phase angles between d' and $\mathbf{G}'$: d' in phase with the maximum upslope pressure gradient (for example, if both occur in midafternoon) and d' leading the upslope pressure gradient by $\frac{1}{6}$ sol. The latter is thought to be somewhat more realistic and corresponds to maximum upslope pressure gradient in the midafternoon and maximum turbulent coupling in the late afternoon. Some sample hodograph results are shown in Figure 13. For the VL-1 site these hodographs have the following properties.

1. Although none of the calculated hodographs resemble the observed VL-1 hodograph in detail, the gross aspects of counterclockwise rotation and correct phase of the upslope wind are reproduced for some values of the parameters.

2. Counterclockwise hodograph rotation occurs only for rather large values of d' ($\gtrsim 0.5 \times 10^{-4}\,\mathrm{s}^{-1}$) and for the case with a $\frac{1}{6}$-sol time lag between the maximum of d' and the maximum upslope pressure gradient.

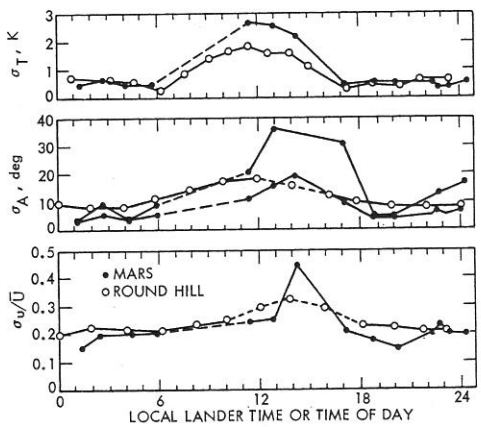

Fig. 12. Comparison of the diurnal variations on Mars (VL-1 sol 29) and Round Hill, Massachusetts: (bottom) gustiness ratio, (middle) standard deviation of wind angle, (top) standard deviation of temperature. In the top plots the terrestrial data have been multiplied by 4 and are derived from an earlier experiment.

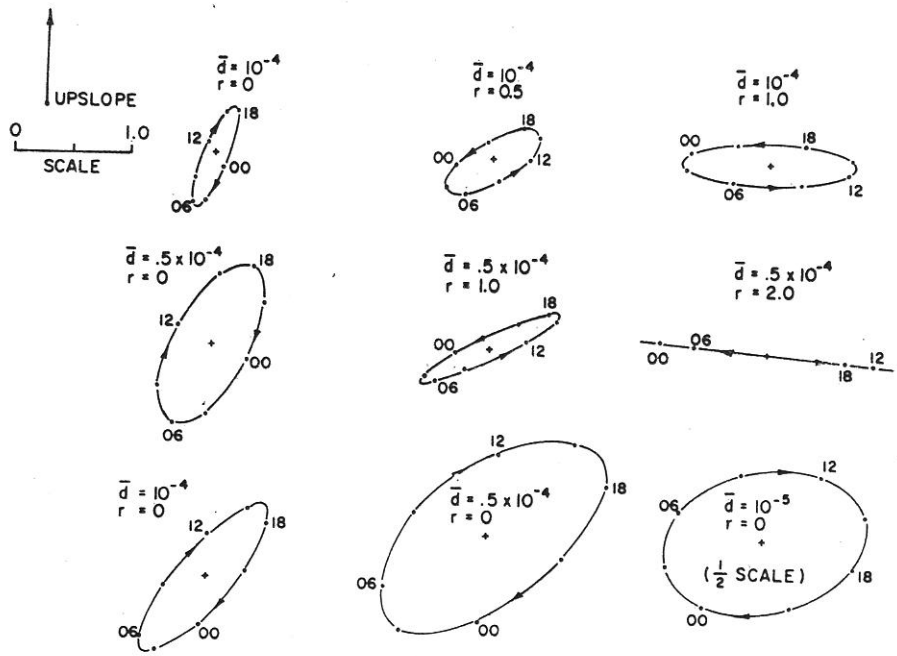

Fig. 13. Sample hodographs computed from (3). The upper six cases are for 23°N; the lower three are for 48°N. The four cases with nonzero coupling to winds aloft ($r \neq 0$) have a ⅛-sol phase lag between the time of maximum coupling (1153 LLT) and the time of maximum upslope pressure gradient (1500 LLT). All values are nondimensionalized by dividing the amplitudes by $f^{-1}|\mathbf{G}|$ and are scaled as indicated except for the hodograph at lower right which is one half the scale of the others.

3. These cases also show very low wind amplitudes, partly as a result of the competition between $\mathbf{G}'$ and $d'(\bar{\mathbf{u}} - \bar{\mathbf{u}}_f)$, which gives out-of-phase forcing.

4. Values of r greater than about 1 yield increasingly large discrepancies between the model and observed times of maximum upslope winds.

5. If the three cases shown in Figure 13 having counterclockwise wind rotation are taken to be representative of a reasonable fit to the VL-1 data, one finds an amplitude of $\mathbf{G}'$ and a corresponding estimate of $h|\Gamma'|$ for the particular slope and latitude of VL-1 from (1). ($|\Gamma'|$ is the amplitude of the diurnal oscillation of lapse rate.) The result is $h|\Gamma'| \sim 2$–3°C. This corresponds, for example, to a lapse rate variation of 1–1.5°C/km through a depth of 2 km. For the VL-2 site we find the following.

1. The predicted phase of $\mathbf{u}'$ disagrees with the observed phase to an increasing degree as $|d'|$ decreases from 10^{-4} s^{-1}.

2. The shapes of the model and observed hodographs agree well when $r = 0$ and $|d'| \approx 0.5 \times 10^{-4}$ to 1×10^{-4} s^{-1}.

3. For these parameters the disagreement in phase between the observed and calculated hodographs is still about 45°; note, however, that the correct phase reference, the upslope direction, is quite uncertain for this site.

4. As $|d'|$ increases beyond 0.5×10^{-4} s^{-1}, the model hodographs become thinner than those observed, and there is no significant improvement in the phase discrepancy.

5. If $r = 0$, $|d'| = \bar{d} = 0.5 \times 10^{-4}$ s^{-1} are taken to be 'best fit' values for the VL-2 data, the corresponding value of $h|\Gamma'|$ which is consistent with the slope obtained from the Mars topographic map (Map M25M 3RMC, prepared by the U.S. Geological Survey for the Viking Program, 1976) is ~4–5°C. This value is in reasonable agreement with the value derived for the VL-1 site.

Although no firm conclusions can be drawn from the above analysis, several results are suggested. The rough qualitative agreement between model and observed winds for similar parameter values at both sites supports the hypothesis that the dominant factors are the local slope pressure gradient and coupling with winds aloft. These are the factors suggested by Blackadar and Holton for diurnal boundary layer wind variations, and they have been developed in some detail for Mars by Gierasch, Blumsack, and Wessel. At the VL-1 site both factors appear to be comparable in magnitude; at the VL-2 site there seems to be no need to invoke coupling to winds aloft. A large damping factor seems to be required, but its value may not be unreasonable for winds within 2 m of the surface. A damping time scale of the order of 4 hours for the surface winds is inferred. Finally, the two hodographs seem to be most consistent with a 'slope heating parameter' $h|\Gamma'| \approx 2$–5°C.

Pressure Models

The repeatable daily pressure variations for the early sols have been analyzed into diurnal and semidiurnal tidal components at both sites [*Hess et al.*, 1976*a*, *b*]. The peak-to-peak amplitudes of the diurnal and semidiurnal components were found to be 0.16 and 0.07 mbar at VL-1, and 0.03 and 0.03 mbar at VL-2. On Mars as on earth the diurnal component may experience substantial regional modulations as a result of interactions with the topography and other spatially variable surface factors. It is also sensitive to details of the vertical thermal structure of the atmosphere [*Zurek*, 1976]. The semidiurnal component of the daily pressure variation on earth shows very little longitudinal dependence and does not seem to be much affected by orography, continent-ocean differences, or vertical structure variations [*Chapman and Lindzen*, 1970], and similar behavior can be expected for the semidiurnal tide on Mars. The reason for this difference in behavior holds on both planets: the predominant semidiurnal tidal modes have a much larger vertical scale than those of the diurnal tide. Consequently, the semidiurnal tide is much less sensitive to the

precise lower boundary condition and to irregularities in heating. The amplitude and phase of the semidiurnal tide should relate in a fairly direct way to the semidiurnal heating. Thus we adopt the following strategy: (1) use the observed properties of the semidiurnal tide at the VL-1 and VL-2 sites to infer some properties of the heating and (2) use these properties to constrain models of the diurnal tide. Only the first of these two steps is attempted here.

Following Chapman and Lindzen, we can express the semidiurnal surface pressure ratio $\delta p/\bar{p}$ in the form

$$\delta p/\bar{p} = \text{Re}\,\{(i\gamma/\omega)\sum_n \theta_n(\phi)Y_n(0)e^{i\omega t}\} \tag{4}$$

where $\gamma = c_p/c_v$ is the ratio of specific heats, ω is the semidiurnal frequency, and $\theta_n(\phi)$ is the nth semidiurnal Hough function, or latitude-dependent modal solution of LaPlace's tidal equation [cf. *Chapman and Lindzen*, 1970]. $Y_n(x)$ is the solution of the vertical structure equation

$$\frac{d^2Y_n}{dx^2} + \lambda_n{}^2Y_n = \frac{(\gamma-1)J_ne^{-x/2}}{\gamma^2gh_n} \tag{5}$$

where x is the vertical coordinate divided by the local scale height H, g is the gravitational acceleration, and J_n is the heating per unit mass in the nth tidal mode. The parameter $\lambda_n{}^2$ is

$$\lambda_n{}^2 = \left[\frac{(\gamma-1)H}{\gamma} + \frac{dH}{dx}\right]\Big/ h_n - \frac{1}{4}$$

where h_n, the 'equivalent depth,' is a separation parameter for the nth mode in LaPlace's tidal equation. We consider the class of heating models considered by *Zurek* [1976].

$$J_n = J_0e^{-(\nu+i\alpha)x} \tag{6}$$

where J_0, ν, and α are constants. The solution to (5) is sought which satisfies the radiation condition $Y_n \to \exp(i\lambda_n x)$ as $x \to \infty$ and which also has vanishing vertical velocity at $x = 0$. The latter condition applied to Y_n takes the form

$$(dY_n/dx) + \beta_nY_n = 0 \qquad x = 0 \tag{7}$$

where $\beta_n = (H/h_n - \frac{1}{2})$.

For the semidiurnal tide in the Mars atmosphere it is sufficient to treat λ_n as a constant. Then the required solution to (5) evaluated at $x = 0$ is

$$Y_n(0) = \{\beta_n[(\nu+\tfrac{1}{2}) + i(\alpha-\lambda_n)] \cdot [1 + i\lambda_n\beta_n{}^{-1}]\}^{-1}\left[\frac{(\gamma-1)J_0}{\gamma^2gh_n}\right] \tag{8}$$

The surface heating rate can be evaluated in terms of the net surface heat flux in the nth semidiurnal mode, F_0:

$$J_0 = \frac{gF_0}{p_s}\cdot\frac{[\alpha^2 + (\nu+1)^2]}{[\nu+1]} \tag{9}$$

where p_s is the mean surface pressure. We also assume that F_0 is a constant fraction A of the total solar flux available in the nth semidiurnal mode at every latitude. Fourier decomposition of the total solar flux then gives

$$F_0 = \frac{2AF_s}{\pi}\int_{-\pi/2}^{\pi/2}\left(\int_0^{t_s}\cos Z\cos 2t\,dt\right)\theta_n(\phi)\cos\phi\,d\phi \tag{10}$$

where Z is the solar zenith angle and F_s is the solar constant. The local time t (relative to local noon) and the time of sunset t_s are measured in radians, and the Hough function normalization has been used:

TABLE 2. Parameters Used in the Calculation of the Semidiurnal Tide

n	h_n, km	λ_n	β_n	$\theta_n(23°\text{N})$	$\theta_n(48°\text{N})$
2	5.56	0.1841	1.6221	0.796	0.185
4	1.49	0.9002	7.4188	0.548	0.6555
6	0.58	1.4400	16.8515	−0.944	1.0255

F_s = 520 W/m², $H(0)$ = 11.80 km, dH/dx = 0.87 km/scale height, P_s/g = 161.3 kg/m², declination of sun = +23°.

$$\int_{-\pi/2}^{\pi/2}\theta_n{}^2(\phi)\cos\phi\,d\phi = 1$$

Equations (4), (8), (9), and (10) combine to give $\delta p/\bar{p}$ in terms of the parameters A, ν, α, the solar constant, and the atmospheric mass (p_s/g), as well as the desired declination and latitude. The lowest even order Hough function mode is the dominant one in the summation of (4), but we have included the first three even modes in this calculation. The corresponding parameters are given in Table 2.

The resulting amplitudes and phases of the semidiurnal tide for various values of ν and α are shown in Figures 14*a* and 14*b*. Phases shown represent the phase advance relative to local noon. The amplitudes have been divided by the unknown fractional absorption A. Figure 15 shows the ratio of amplitudes at the VL-1 and VL-2 sites predicted by the model. The observed phases reported by *Hess et al.* [1976*a*, *b*] are recapitulated in Table 3. Comparing the observations in Table 3 with the model results, we conclude that reasonable agreement can be achieved with $A \sim 0.1$, $\alpha \sim 1$–2, and essentially any positive value of ν. The general agreement of the ratio of amplitudes at both sites with the model for most values of ν and α, as well as the phase consistency at the two sites lends credence to the model, although a slight phase advance of the pressure at VL-2 relative to VL-1 is predicted in all cases, while a slight phase retardation is actually observed.

The required value of A is quite large, a reflection of the fact that the observed semidiurnal pressure oscillation is itself large. It is unlikely that such a large solar heat input could be accomplished by convective transport from the surface alone. For example, at the latitude of the VL-1 site the maximum daily flux of heat into the atmosphere would have to be of the order of 50 W/m² to produce the observed semidiurnal tide. But the actual heat flux F can be estimated from the bulk transfer relation

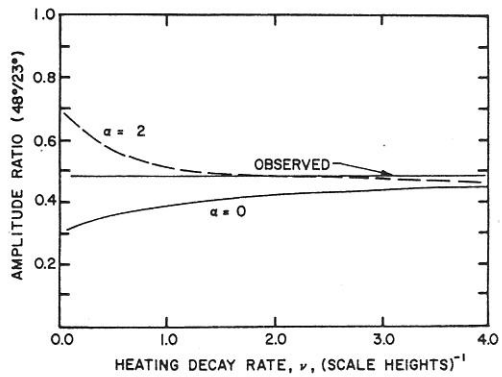

Fig. 14*a*. Dependence of the amplitude of the semidiurnal pressure ratio on ν, the inverse vertical scale of heating, for two values of α, the heating phase lag parameter. The solid lines are for $\alpha = 0$, and the dashed lines are for $\alpha = 2$. Values of $\delta p/\bar{p}$ shown are divided by the absorption parameter A.

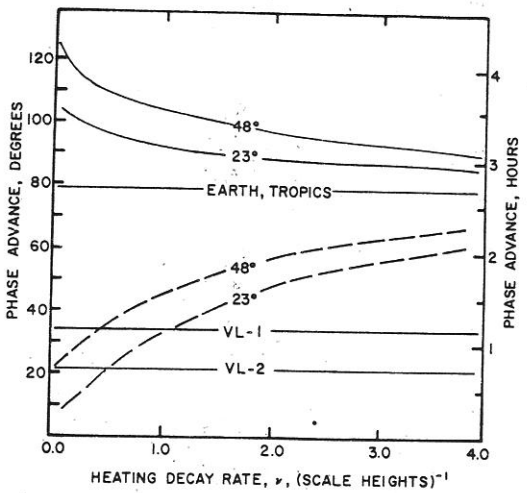

Fig. 14*b*. Dependence of the semidiurnal phase advance, relative to local noon, on ν for two values of α. The solid lines are for $\alpha = 0$, and the dashed lines are for $\alpha = 2$. The observed lags at VL-1 and VL-2 and in the earth's tropics are also shown.

$$F_c = \rho C_p C_D u \Delta T \tag{11}$$

where the transfer coefficient $C_D \approx [k_0/\ln(z/z_0)]^2$; k_0 is von Karman's constant, z is instrument height (1.6 m), and z_0 is roughness length (estimated to lie in the range 0.01–1 cm). Other parameters are the measured wind u and the temperature difference ΔT between the atmosphere at instrument height and the ground. The latter can be estimated with the aid of ground temperatures inferred from the Viking orbiter infrared experiment [*Kieffer et al.*, 1976]. Rough evaluations give F_c of about 10 W/m² at the VL-1 site. Although this may be underestimating the global average of F_c, it is very unlikely to be in error by as much as a factor of 3. Since convection alone does not seem adequate to provide the required heating, absorption of solar radiation must be playing an important role. It appears that absorption of solar radiation is providing at least half of the required heating. The absorbing agent is apparently atmospheric dust. The opacity due to dust has been monitored by the imaging systems on both landers, and the optical depths for normal incidence measured during this period were substantial, ranging from 0.2 to 0.4 [*Mutch et al.*, 1976*c*; *Pollack et al.*, 1977].

Even though radiation absorption must provide an important thermal drive, convective heating also appears to be playing a role. Radiation absorption alone should exhibit very little phase variation with height, with maximum heating near local noon. This would produce a semidiurnal pressure maximum very near to 0850 LLT (+90° phase shift; see Figure 14). Such a phase shift is observed for the semidiurnal tide on earth which is known to be driven primarily by radiation [cf. *Chapman and Lindzen*, 1970]. The observed Martian pressure phases indicate that the heating maximum occurs considerably later than noon at some levels in the atmosphere. Such a phase retardation of heating is expected at levels above the surface for convective heating. We conclude that both factors, convection and absorption of solar radiation, play significant roles in driving the global tides.

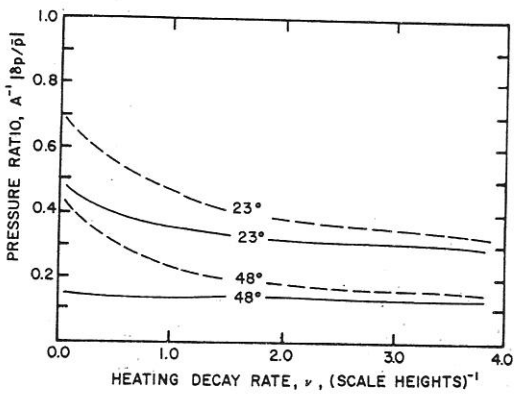

Fig. 15. Dependence of the ratio of the semidiurnal amplitudes at the VL-2 and VL-1 latitudes on ν and α. The solid lines are for $\alpha = 0$, and the dashed lines are for $\alpha = 2$.

TABLE 3. Observed Tidal Properties on Mars

	VL-1	VL-2	(VL-1)/(VL-2)
Amplitude ratio	0.0050	0.0022	0.44
Phase, hours	1.17	0.75	

The absorption fraction estimated from the semidiurnal tidal model can be used to estimate an effective diurnal temperature change for the equatorial atmosphere. For example, values $A = 0.1$, $\nu = 2$ imply an average daily temperature amplitude of 10°C through a layer 5 km deep. Although this variation is quite large, so far as we know it is not inconsistent with any other data. It is much larger than the temperature variations which were required to drive the boundary layer winds, but the boundary layer winds are likely to reflect primarily the convective contribution to heating. We note that the inferred values of $h|\Gamma'|$ are quite consistent with the convective heating estimate at the VL-1 site from (11). Moreover, the apparent requirement of a phase lag between the time of maximum thermal drive for these winds and the time of maximum vertical coupling is consistent with convective driving. The boundary layer winds are probably not very responsive to radiative heating through a deep layer.

SEASONAL VARIATION OF PRESSURE

We have previously reported [*Hess et al.*, 1976*a*, *b*] a secular decline of the sol mean pressure at the two lander sites. When initially detected at VL-1, this decline was at the rate of 0.0122 mbar per sol or 0.16% per sol, a rapid rate of the sort that is never seen on earth. Although we did not believe that this was due to a defective instrument, that possibility could not then be ruled out. When VL-2 landed, it too showed a long-term decrease in pressure, thus making it still more unlikely that an instrumental problem was the cause. We now have a long enough run of data to demonstrate that a minimum has been reached and that the pressure is rising. This makes it quite certain that we are dealing with a real physical process and not with instrumental anomalies.

The sol mean pressure results from both landers are given in Figure 16, extending well past the end of the nominal mission. The minima are quite broad, and it is impossible to specify the date of minimum with great accuracy. However, the data indicate that the time of minimum pressure is the same at both landers and is approximately VL-1 sol 100 (VL-2 sol 56), or $L_s = 149°$. The uncertainty in this seems to be ±10 sols or ±5° of L_s.

The obvious interpretation of these results is the loss of atmospheric mass through condensation of CO_2 on the winter

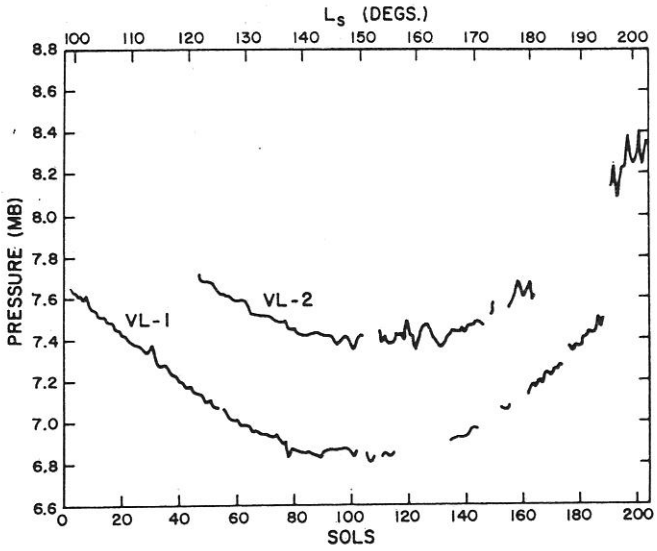

Fig. 16. Surface atmospheric pressures averaged over each sol for VL-1 and VL-2, plotted as a function of time (VL-1 sols) and L_s. Gaps are due to missing data or to data that have not yet been reduced.

(southern) cap and the subsequent gain of atmospheric mass through sublimation of CO_2 from that cap when the season progresses sufficiently. A seasonal variation of atmospheric pressure was anticipated before the Viking landers touched down [*Leighton and Murray*, 1966; *Briggs*, 1974; *Dzurisin and Ingersoll*, 1975; *Pollack et al.*, 1976]. As we have previously reported [*Hess et al.*, 1976*a*], the results of Pollack et al., based upon a numerical general circulation model for the Viking season, gave a nearly exact fit to the initial rate of decrease found at VL-1. Briggs' calculation resulted in a rate of change of pressure that was some 25% too slow. This discrepancy is understandable because Briggs' model constrained the edge of the polar cap to lie no further equatorward than 57°S, in agreement with the best data then available. Pollack et al. placed no such constraint on the cap but allowed it to grow as dictated by the model physics. Viking orbital pictures indicate that the southern cap does extend farther north than 57°S, so that the choice made in the general circulation model was probably better. The additional condensation of CO_2 involved in a cap extending equatorward of 57°S is probably responsible for the excellent agreement between the general circulation model and the observed rate of change of pressure during the early part of the VL-1 mission.

For the very practical reason that general circulation models consume large amounts of computer time, Pollack et al. did not calculate results as the season changed but obtained predictions for only one value of L_s. Thus we have not as yet had the capability to compare the full range of observed data to the most successful model. The portion of the seasonal curve given in Figure 14 can be compared to the results of Briggs, which do not include any sorption of CO_2 on the regolith, and to those of Dzurisin and Ingersoll, which do include plausible parameterized interactions with the regolith. Since sorption on the regolith would buffer the exchange of mass between atmosphere and cap, its effect would be to decrease the amplitude of the pressure curve and to shift the extrema to earlier times. Thus Dzurisin and Ingersoll predict a rate of change of pressure that is 70% slower than is observed. This discrepancy suggests that the CO_2 sorption mechanism is not significant on a seasonal time scale. However, the time of occurrence of minimum pressure from Figure 14 is appreciably closer to the time predicted when sorption is included (Dzurisin and Ingersoll) than to that predicted when sorption is omitted (Briggs). Thus amplitude considerations argue against the importance of CO_2 sorption, while phase considerations favor it.

It is likely that this contradiction may be another consequence of the artificial restriction of the edge of the cap to poleward of 57°S in the Briggs model. The condensate that actually deposits equatorward of that latitude would be the first to sublime and could be responsible for the early occurrence of the minimum without the intervention of a sorption mechanism. The Leighton-Murray model, which had no restrictions on the latitude of the cap edge, is in good agreement with our observations. This suggests that the above analysis is correct.

It should be mentioned that adsorption of CO_2 on the regolith is potentially significant for the important issue of climatic changes on Mars. For cyclic climate change to occur it is necessary to have a reservoir into and out of which large amounts of CO_2 (or some other gas) can pass. Prior to Viking it was supposed that the residual summer polar cap was condensed CO_2 and that it was the needed reservoir [*Ward et al.*, 1974]. Viking orbital infrared measurements have demonstrated that the residual northern polar cap is too warm to contain condensed CO_2 in equilibrium with the atmosphere [*Kieffer et al.*, 1976] and therefore cannot serve as a reservoir for atmospheric CO_2. The same conclusion is probably applicable to the southern cap. Therefore the idea that appreciable CO_2 can be stored by adsorption in the regolith [*Fanale and Cannon*, 1974] supplies the only other reasonable reservoir. If it ultimately develops that the seasonal pressure variation requires sorption of CO_2, that would be powerful support for the idea of the regolith as a storehouse for CO_2. If the reverse conclusion is drawn, it will weaken the idea somewhat, but not fatally, because the process could conceivably be insignificant on the scale of 1 year but significant on a scale of thousands or millions of years.

For the range of L_s represented in Figure 14 there is probably little or no contribution from the northern cap. At the beginning of the Viking missions that cap likely had no CO_2 left in it, and the contributions to atmospheric mass by H_2O are insignificant. For the latest dates represented in Figure 14, little if any CO_2 could have been condensed on the northern cap. Thus we probably have seen only the consequences for total atmospheric pressure of the southern cap. Subsequent data will reveal the full interplay of the atmosphere with both caps.

Solar Conjunction and Extended Mission

The two Viking landing sites were deliberately selected so that (among many other criteria) expected wind speeds would be low during landing and the primary mission. This has been found to be the case, and the wind behavior has been quite regular throughout northern summer, particularly at the near-equatorial VL-1 site. Temperatures have also been mild by Martian standards, and very little secular change was observed. In fact, the most striking aspect of Martian weather has been its remarkable regularity. The only notable departures have been the secular pressure decrease and the wind event at the VL-2 site.

The primary mission ended early in November 1976, with the beginning of the solar conjunction period. Meteorological data were taken throughout this period and stored on the onboard tape recorder for postconjunction transmission to earth.

Tape recorder capacity limited the amount of data to 16 wind and temperature samples each 1½ hours during the night, 32 each 1½ hours during the day, and a pressure sample every 17 min. This was sufficient to maintain a continuous record of the diurnal cycle and pressure trends at both sites. An increase in wind variability was observed at the VL-2 site with continued temperature decrease. However, conditions at the VL-1 site remained essentially the same as before. Pressure began a slow rise at both sites.

It is planned to operate the meteorology experiment for nearly 2 earth years in order to cover all four seasons on Mars. With the establishment of this extended mission we have been able to return to quasi-continuous sampling and expect to remain in this mode. Measurements will be coordinated with lander imaging and the orbital experiments. Northern autumn began in early January 1977, and perihelion will occur in late April 1977, northern winter beginning on May 30, 1977 (L_s = 270°). We expect to see some dramatic meteorological changes during this period. During northern autumn, and more certainly by the time of perihelion, high winds, possibly in excess of 50 m s^{-1}, should occur. These should be accompanied by blowing sand and dust, both locally and globally. Associated with these could be local and meso-scale vortex systems. Additionally, frontal systems are believed to occur [*Briggs and Leovy*, 1974]. Evidence for the occurrence of at least some of these phenomena comes from a long history of earth-based observations, from the Mariner and Viking orbiters, and from the Viking landers. For example, lee deposits of granular material are present at both landing sites, indicating deposition by strong northeast winds at VL-1 and northwest winds at VL-2. These directions are opposite to those of the maximum winds observed during the primary mission (southwest at VL-1 and southeast at VL-2). To date, in the extended mission we have already noted significant changes in wind behavior from the summer pattern. A series of events with moderate (10–15 m s^{-1}) winds from northerly directions has occurred at VL-2. Some events have been associated with temporary temperature decreases superimposed upon the general temperature decline. These events are suggestive of cold front passages. Temperature at VL-2 is decreasing at an accelerating rate with minima as low as 165°K now being observed. The seasonal effect at the VL-1 site, however, continues to be small. Details of these observations will be presented when data reduction and analysis are completed.

Continued large pressure variations are expected as the CO_2 polar caps form and sublimate. Monitoring of pressure throughout the Martian year should allow determination of CO_2 behavior, particularly with respect to the amounts deposited at, and cycled between, the polar caps. It is possible that CO_2 condensation may occur at the VL-2 site during northern winter, and temperature measurements will be important in the study of the condensation-sublimation behavior. In this regard we have found, during the primary mission at both VL-1 and VL-2 sites, a suggestion that the temperature sensors are detecting the H_2O frost point. This is indicated by a temporary decline in the nocturnal rate of decrease of temperature, occurring in the time period 0100–0300 LLT and at temperatures of about 191°K (VL-1) and 196°K (VL-2). Such an effect could be caused by the formation of a ground ice fog acting to decrease the rate of surface radiative loss to a small extent. Much more work is required to verify this; hence these data are not presented here. However, it is worth noting that observations by *Pollack et al.* [1977] indicate the possible presence of nocturnal ice fog. If we are indeed detecting the frost point, then such data combined with the observations of *Farmer et al.* [1977] can provide a basis for modeling the vertical distribution of water vapor and its seasonal behavior. Following temperature and wind trends will allow verification (and modification) of circulation and surface thermal models. Seasonal variations in the diurnal and semidiurnal pressure oscillations will allow us to monitor the atmospheric tidal responses and their thermal drives.

The most interesting meteorology lies ahead, and we expect that the meteorological sensors will survive throughout the extended mission and beyond.

Acknowledgments. The section of this paper on interpretation of the daily variations of wind and pressure has benefited from discussions with R. Zurek, J. M. Wallace, H. Tennekes, and S. Mullen. We are indebted to T. Chamberlain, H. Cole, R. Dutton, G. Greene, J. Mitchell, and W. Simon, without whose devoted efforts this work would not have been possible. This research was supported by the National Aeronautics and Space Administration under contract NASI 9693, NASI 11854, and NASI 9694.

REFERENCES

Blackadar, A. K., Boundary layer wind maxima and their significance for the growth of nocturnal inversions, *Bull. Amer. Meteorol. Soc., 38,* 283, 1957.

Blumsack, S. L., P. J. Gierasch, and W. R. Wessel, An analytical and numerical study of the Martian planetary boundary layer over slopes, *J. Atmos. Sci., 30,* 66, 1973.

Briggs, G. A., The nature of the residual Martian polar caps, *Icarus, 23,* 167, 1974.

Briggs, G. A., and C. B. Leovy, Mariner 9 observations of Mar's north polar hood, *Bull. Amer. Meteorol. Soc., 55,* 278, 1974.

Chamberlain, T. E., H. L. Cole, R. G. Dutton, G. C. Greene, and J. E. Tillman, Atmospheric measurements on Mars: The Viking meteorology experiment, *Bull. Amer. Meteorol. Soc., 57,* 1094, 1976.

Chapman, S., and R. S. Lindzen, *Atmospheric Tides*, Gordon and Breach, New York, 1970.

Cramer, H. E., F. A. Record, and J. E. Tillman, Investigation of low level turbulent structure for various roughnesses and gross meteorological circulations, final report, U.S. Army contract DA49-092-ARO-66, Dep. of Meteorol., Mass. Inst. of Technol., Cambridge, 1967. (Available from J. E. Tillman, Department of Atmospheric Sciences, University of Washington, Seattle, Washington 98105.)

Dzurisin, D., and A. P. Ingersoll, Seasonal buffering of atmospheric pressure on Mars, *Icarus, 26,* 437, 1975.

Fanale, F. P., and W. A. Cannon, Exchange of adsorbed H_2O and CO_2 between the regolith and atmosphere of Mars caused by changes in surface insolation, *J. Geophys. Res., 79,* 3397, 1974.

Farmer, C. B., D. W. Davies, A. L. Holland, D. D. LaPorte, P. E. Doms, Mars: Water vapor observations from the Viking orbiters, *J. Geophys. Res., 82,* this issue, 1977.

Gierasch, P. J., and R. M. Goody, A study of the thermal and dynamical structure of the Martian lower atmosphere, *Planet. Space Sci., 16,* 615, 1968.

Hess, S. L., R. M. Henry, J. Kuettner, C. B. Leovy, and J. A. Ryan, Meteorology experiments: The Viking Mars lander, *Icarus, 16,* 196, 1972.

Hess, S. L., R. M. Henry, C. B. Leovy, J. A. Ryan, J. E. Tillman, T. E. Chamberlain, H. L. Cole, R. G. Dutton, C. G. Greene, W. E. Simon, and J. L. Mitchell, Mars climatology from Viking after 20 sols, *Science, 194,* 78, 1976*a*.

Hess, S. L., R. M. Henry, C. B. Leovy, J. L. Mitchell, J. A. Ryan, and J. E. Tillman, Early meteorological results from the Viking 2 lander, *Science, 194,* 1352, 1976*b*.

Holton, J. R., The diurnal boundary layer wind oscillation above sloping terrain, *Tellus, 19,* 199, 1967.

Kieffer, H. H., Soil surface temperatures at the Viking landing sites, *Science, 194,* 1344, 1976.

Kieffer, H. H., S. C. Chase, T. Z. Martin, E. D. Miner, and F. D. Palluconi, Martian north pole summer temperatures: Dirty water ice, *Science, 194,* 1341, 1976.

Leighton, R. B., and B. C. Murray, Behavior of carbon dioxide and other volatiles on Mars, *Science, 153,* 136, 1966.

Mutch, T. A., A. B. Binder, F. O. Huck, E. C. Levinthal, S. Liebes, E. C. Morris, W. R. Patterson, J. B. Pollack, C. Sagan, and G. R. Taylor, The surface of Mars: The view from the Viking 1 lander, *Science, 193,* 791, 1976*a*.

Mutch, T. A., et al., The surface of Mars: The view from the Viking 2 lander, *Science, 194,* 1277, 1976*b*.

Mutch, T. A., R. E. Arvidson, A. B. Binder, F. O. Huck, E. C. Levinthal, S. Liebes, E. C. Morris, D. Nummedal, J. B. Pollack, and C. Sagan, Fine particles on Mars: Observations with the Viking 1 lander cameras, *Science, 194,* 87, 1976*c*.

Pollack, J. B., C. B. Leovy, Y. H. Mintz, and W. Van Camp, Winds on Mars during the Viking season: Predictions based on a general circulation model with topography, *Geophys. Res. Lett., 3,* 479, 1976.

Pollack, J. B., D. Colburn, R. Kahn, J. Hunter, W. Van Camp, C. E. Carlston, and M. R. Wolfe, Properties of aerosols in the Martian atmosphere as inferred from Viking lander imaging data, *J. Geophys. Res., 82,* this issue, 1977.

Seiff, A., D. B. Kirk, and R. Blanchard, The Viking atmospheric structure experiment: Preliminary results, paper presented at the annual meeting of the Division of Planetary Sciences, Amer. Astron. Soc., Honolulu, Hawaii, Jan. 1977.

Tillman, J. E., The indirect determination of stability, heat and momentum fluxes in the atmospheric boundary layer from scalar variables during dry unstable conditions, *J. Appl. Meteorol., 11,* 783, 1972.

Wallace, J. M., and F. R. Hartranft, Diurnal wind variations: Surface to 30 km, *Mon. Weather Rev., 96,* 446, 1969.

Ward, W. R., B. C. Murray, and M. C. Malin, Climatic variations on Mars, 2, Evolution of carbon dioxide atmosphere and polar caps, *J. Geophys. Res., 79,* 3387, 1974.

Zurek, R. W., Diurnal tide in the Martian atmosphere, *J. Atmos. Sci., 33,* 321, 1976.

(Received March 28, 1977;
revised May 26, 1977;
accepted May 26, 1977.)